Received: 13 November 2019 | Revised: 29 March 2020 | Accepted: 4 April 2020

DOI: 10.1002/jbm.a.36989

ORIGINAL ARTICLE

Society For Biomaterials | WILEY

Collagen membranes of dermal and pericardial origin—In vivo evolvement of vascularization over time

Michael Dau[1] | Lisann Volprich[1] | Eberhard Grambow[2] | Brigitte Vollmar[3] | Bernhard Frerich[1] | Bilal Al-Nawas[4] | Peer W. Kämmerer[1,4]

[1]Department of Oral, Maxillofacial Plastic Surgery, University Medical Center Rostock, Rostock, Germany

[2]Department for General-, Visceral-, Vascular- and Transplantation Surgery, University Medical Center Rostock, Rostock, Germany

[3]Institute for Experimental Surgery, University Medical Center Rostock, Rostock, Germany

[4]Department of Oral, Maxillofacial Plastic Surgery, University Medical Center Mainz, Mainz, Germany

Correspondence
Peer W. Kämmerer, Department of Oral, Maxillofacial Plastic Surgery, University Medical Center Mainz, Augustusplatz 2, 55131 Mainz, Germany.
Email: peer.kaemmerer@unimedizin-mainz.de

Funding information
DGI (Deutsche Gesellschaft für Implantologie im Zahn-, Mund- und Kieferbereich e.V., Munich, Germany)

Abstract

Aim of the study was to compare the evolvement of vascularization over time of collagen membranes (CMs) of dermal and pericardial origin in an in vivo animal study. Twenty-eight mice underwent implantation of three commercially available CM derived from porcine dermis (homogenous structure: CM1 (Control 1) and bilayer structure: CM2 [Control 2]), from porcine pericardium (CM3; Test 1) as well as CM3 sprayed with silica-enhanced nanostructured hydroxyapatite (CM4, Test 2). After 3, 6, 9, and 12 days, intravital fluorescence microscopy was conducted for determination of capillary diameter, density, flow, and length. At Day 12, samples were examined immunohistologically for expression of fibroblast growth factor receptor 4 (FGFR4), CD11b, CD68, αSMA, and CD34. In all CM, intravital fluorescence microscopy over time showed increasing values for all parameters with the highest levels in CM4 and the lowest values in CM1. Significant lower amounts of FGFR4, CD11b, and CD68 were detected in CM4 when compared to CM2 ($p < .05$). In contrast to CM3, lower values of αSMA and higher numbers of CD34 positive-marked vessels were observed in CM4 ($p < .05$). In conclusion, dermal bilayer as well as pericardial CM seem to have a higher vascularization rate than dermal homogenous CM. Additional coating of pericardial CM with a silica-enhanced hydroxyapatite increases the speed of vascularization as well as biological remodeling processes.

KEYWORDS

angiogenesis, collagen membrane, dermal, dorsal skinfold chamber, guided bone regeneration, nanocrystalline hydroxyapatite, pericardial, silicon dioxide, vascularization

1 | INTRODUCTION

Guided bone regeneration (GBR) is a commonly used procedure for regeneration of osseous defects of the jaws. Here, nonresorbable and resorbable barrier membranes are thought to exclude nonosteogenic tissue and to stabilize the grafted defect (Elgali, Omar, Dahlin, & Thomsen, 2017; Kämmerer et al., 2017). Nonresorbable membranes have to be removed during a second surgical intervention and are susceptible to higher complication rates in terms of premature exposure and infection (Chiapasco & Zaniboni, 2009), that could be caused by lack of vascular supply through the membrane (Elgali et al., 2017). Especially for horizontal defects, resorbable collagen-based membranes (CM) offer similar clinical success but less complication rates plus degradation within the host tissue (Keestra, Barry, Jong, & Wahl, 2016; Naenni et al., 2017; Pabst & Kämmerer, 2020). Besides, experimental findings suggest that CM may also have an active role in promoting osseous regeneration next to the passive barrier function (Elgali et al., 2017; Liu & Kerns, 2014). For example, the overlying CM may have an additional influence on graft

vascularization that is known to have a pivotal role for successful tissue integration (Koerdt, Ristow, Wannhoff, Kubler, & Reuther, 2014). In accordance, improvement of vascularization of CM could be of high interest. As CMs are derived from different tissues and their degradation as well as tissue integration depends on the source (e.g., dermis and pericardium) (Bunyaratavej & Wang, 2001), it is possible than they have a different biological behavior over time that has not been evaluated so far.

Further modification of CM with enamel matrix, respectively, platelet-rich fibrin resulted in a significantly enhanced migration of endothelial cells (Park et al., 2018) and an increased angiogenesis (Blatt et al., 2020). A combination of CM with recombinant platelet-derived growth factor increased early bone growth in a rabbit model (Kämmerer et al., 2013) and improved soft tissue healing (Amorfini, Migliorati, Signori, Silvestrini-Biavati, & Benedicenti, 2014). However, also membranes for GBR modified with incorporated bone substitute materials (BSMs) such as hydroxyapatite or beta-tricalcium phosphate have shown to promote the activity of stromal and osteoblastic cells both in vitro and in vivo (Li et al., 2011; Shim et al., 2013; Teng et al., 2009). Besides, the BSM allows the membrane to withstand static pressure to a greater extend (Anderud et al., 2014).Though, there are also vast differences regarding the biological behavior of BSM (Dau et al., 2016; Kyyak et al., 2020). For example, synthetic silicium dioxide-enhanced nanostructured hydroxyapatite seems to have a high biocompatibility and vascularization rate in vitro and in vivo (Abshagen, Schrodi, Gerber, & Vollmar, 2009; Ghanaati et al., 2013) and could be an interesting candidate for additional coating of a CM.

Regardless the observed differences in vascularization of various CM, most study results based on histomorphometric analyses (Ghanaati, 2012; Rothamel et al., 2005; Rothamel et al., 2014; Schwarz, Rothamel, Herten, Sager, & Becker, 2006; Silva et al., 2017) at defined time points using a combination of light microscopy and immunohistochemical staining. Intravital fluorescence microscopy in a dorsal skin fold chamber model (Sckell & Leunig, 2009; Sckell & Leunig, 2016) provides in vivo analyses of vascularization including the evolvement over time.

Therefore, the aim of this study was to investigate and compare vascularization parameters of CM of porcine dermal and pericardial origin using intravital fluorescence microscopy over time and final (immuno)histomorphometry using an in vivo dorsal skin fold mouse model. In addition, a pericardial CM additionally sprayed with synthetic silicium dioxide-enhanced nanostructured hydroxyapatite was tested. The null hypothesis was that there are no differences in vascularization over time as well as at the final endpoint between the different CMs.

2 | MATERIALS AND METHODS

2.1 | Study materials

Four different porcine CMs, two of dermal origin and two of pericardial origin, were used in the experiment:

- CM1 (CollProtect, Botiss biomaterials GmbH, Zossen, Germany) is derived from porcine dermis and consists of a homogenous, dense and porous 3D network of collagen bundles.
- CM2 (Bio-Gide, Geistlich Pharma AG, Wolhusen, Switzerland), also from porcine dermal origin, has a bilayer structure consisting of a compact outer layer and a porous inner layer of collagen fiber bundles.
- CM3 (Jason, Botiss biomaterials GmbH) originates from porcine pericardium and consists of differently orientated collagen fibers.
- CM4 consists of the porcine pericardium membrane CM3 that was additionally sprayed with a silicium dioxide-enhanched nanostructured synthetic hydroxyapatite (NanoBone S39, Artoss GmbH, Rostock, Germany). For this purpose, the spin-spray coating was conducted using a custom-made two-substance nozzle in a laminar flow box (Herasafe HSP12 Safety Cabinets class 2, Kendro Laboratory Products GmbH, Hanau, Germany) with a coating time of 0.5 s. Subsequently, the sprayed membranes were dried under oil-free airflow as described before (Adam et al., 2014).

2.2 | Animal model and procedures

An established animal mouse dorsal skinfold chamber model was used in the present study. The experiment was approved by the State Office of Agriculture, Food Safety and Fishery Mecklenburg-Vorpommern, Germany (LVL M-V/TSD/7221.3–1.1-040/16) and followed the National Institutes of Health guidelines for the care and use of laboratory animals as well the ARRIVE Guidelines for Reporting Animal Research (Kilkenny, Browne, Cuthill, Emerson, & Altman, 2010). Twenty-eight male C57BL/6 Tyr mice underwent implantation of different CMs in a dorsal skinfold chamber (Figure 1a). The animals were kept in a room with 12/12 hr dark light cycle with food and water ad libitum. The mice were postoperatively kept alone in type III cages and enrichment was provided by paper role and rodent wood. All performed surgical interventions were conducted under general anesthesia with an intramuscular injected mixture of 90 mg ketamine hydrochloride (Ketamin 10%, Belapharm, Vercha, Germany) and 25 mg xylazin hydrochloride (Rompun 2%, Bayer HealthCare Animal Health, Leverkusen, Germany) per 1 g animal body weight. Following anesthesia and shaving of the dorsal skin, a double skin layer was formed and fixed on a titanic frame as described in the literature (Sckell & Leunig, 2009; Sckell & Leunig, 2016). A skin defect was created using microsurgical instruments and a surgical light microscope on a tabletop (M 651 MSD, Leica Microsystems, Wetzlar, Germany). Cutis, subcutis, musculus panniculus carnosus, and the retractor muscles were removed. Afterward, the cover glasses of the dorsal skinfold chamber were placed under constant rinsing with sodium chloride solution to avoid entrapped air. Metamizol natrium (Novaminsulfon-ratiopharm, ratio-pharm GmbH, Ulm, Germany) was applied in the drinking water on a daily base preoperatively and postoperatively. After 3 days, 4×4 mm^2 large pieces of the CM were randomly selected (achieved by using a computer-generated list) and placed onto the dorsal skinfold chamber area in general anesthesia. Following the reclosure of the dorsal skinfold chamber, first intravital fluorescence microscopy images were taken using a fluorescence microscope (Axiotech Vario 100, Zeiss, Oberkochen, Germany; Plan-

NEOFLUAR ×20/0.50 W; Zeiss) after retrobulbar injection of fluorescein isothiocyanate-dextran (2% FITC-Dextran average mol wt 150,000 D, Sigma-Aldrich, Taufkirchen, Germany). All images were captured with a video camera (FK 6990 IQ-S, Pieper, Schwerte, Germany) connected to a S-VHS recorder (AG-7350; Panasonic Germany, Hamburg, Germany) and saved using a DVD recorder (DMR-EX99V, Panasonic Germany). For each sample, 12 predefined regions around the CMs were selected (Figure 1b) and short video sequences (20 s each) were recorded. Here, the vascularization parameters "capillary diameter" (CDI; in μm), "capillary density" (CDE, cm of capillary length [CLE] per predefined area [cm/cm^2]), "capillary flow" (CFL; using the line shift diagram method (De Vriese et al., 2000; Klyscz, Junger, Jung, & Zeintl, 1997) and described in mm per second [mm/s]) and CLE (in μm) were calculated using an image analyzing software (CapImage, Version 8.0, Dr. Zeintl, Heidelberg, Germany). Intravital fluorescence microscopy analyses (Figure 2a,b) were performed on Days 3, 6, 9, and 12. The animals were sacrificed after 12 days, following an intramuscular injection of 360 mg ketamine hydrochloride (Ketamin 10%, Belapharm) and 100 mg xylazin hydrochloride (Rompun 2%, Bayer HealthCare Animal Health) per 1 g animal body weight and the skin in the chamber was harvested. The skin was fixed in 4% phosphate-buffered formalin for 2 days and subsequently dehydrated using an ascending ethanol order with xylene. The dehydrated specimens were embedded in paraffin and 3 μm sections were cut and stained with hematoxylin-eosin (HE) for standard histological analysis. Additionally, sections were subsequently dehydrated using an ascending ethanol order with xylene. To reduce background staining, the endogenous peroxidase of the cells was blocked by using a solution of 194 ml methanol and 6 ml 30% hydrogen peroxide. After rinsing with tris buffered saline solution (TBS), the sections for CD34 (a standard surface protein on endothelial cells) staining were treated with citrate puffer (pH = 6), while specimens for αSMA (smooth muscle actin alpha), respectively, CD68 (a standard surface protein on macrophages) were treated with trypsin/EDTA. The CD11b

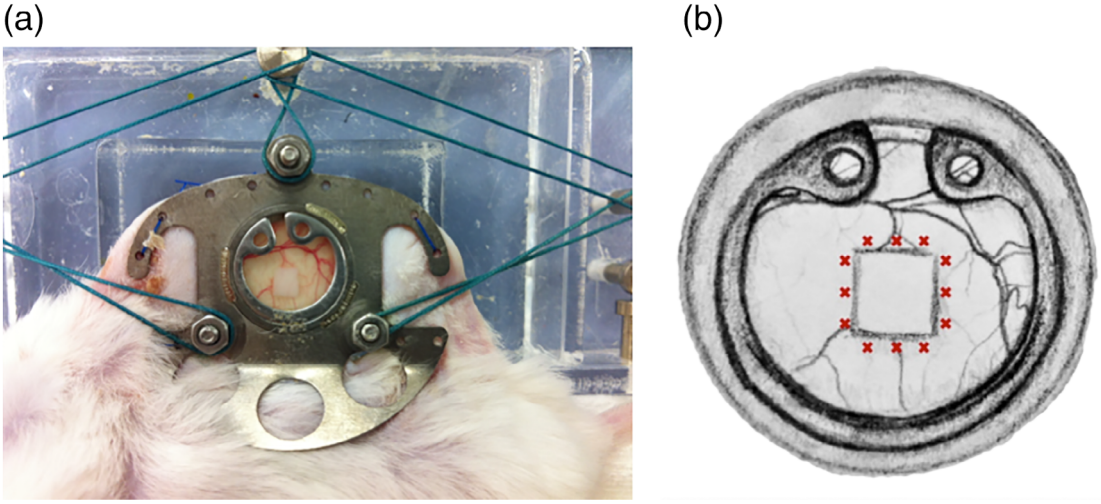

FIGURE 1 Dorsal skinfold chamber (a) and predefined regions of interest surrounding the collagen membrane (b)

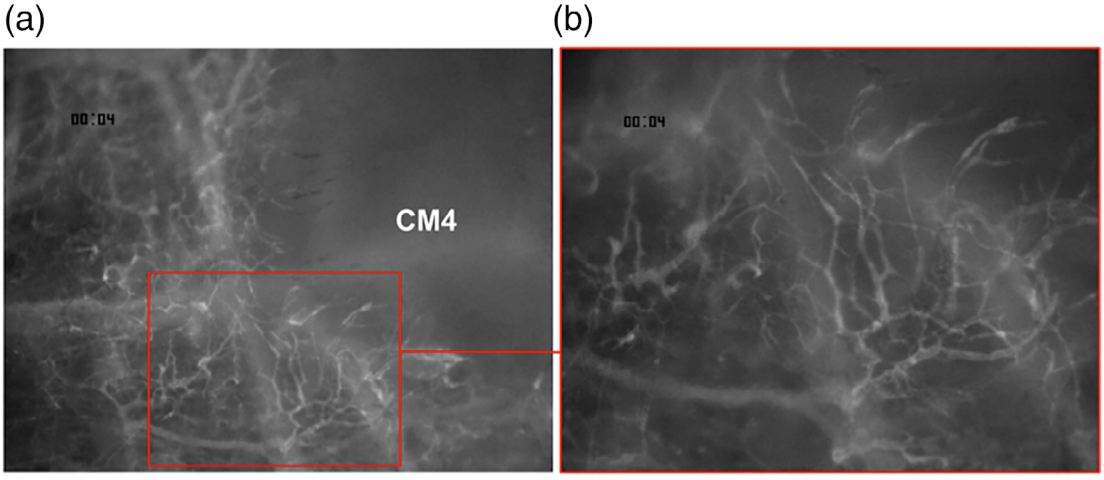

FIGURE 2 Intravital fluorescence microscopy images of a porcine pericardial membrane sprayed with a bone substitute material at Day 9 (a—×5 magnification; b—×10 magnification)

(a standard surface protein on monocytes) and Fibroblast growth factor receptor 4 (FGFR4) staining required no antigen demasking. After rerinsing with TBS, all sections were blocked using bovine serum albumin. Depending on the antibody markers, the sections were incubated with the respective antibodies for detection of CD68 (Anti-CD68 antibody 1:200, Abcam, Cambridge, UK), CD11b (Anti-CD11b antibody 1:250, Abcam), CD34 (Anti-CD34 antibody 1:200, Abcam), αSMA (Anti-alpha smooth muscle Actin antibody 1:500, Abcam), and FGFR4 (Anti-FGFR4 antibody 1:50, Abcam) and rinsed again with TBS. Following incubation of the slides in a humidity chamber, another rerinsing with TBS was performed and in preparation of the antibody linking, all sections were incubated for 30 min with horseradish peroxidase (Labeled Polymer-HRP, EnVision Kit, Dako/Agilent Technologies, Santa Clara, CA). After rinsing with TBS, diaminobenzidine staining and rerinsing with TBS, the sections were counterstained with hemalaun. Using an ascending ethanol order and xylene, all sections were dehydrated and the slides were covered with a rapid mounting medium for microscopy (Entellan, Sigma-Aldrich, St. Louis, MO).

2.3 | Histological analysis

Histological analysis was performed using a light microscope (Axio Imager.M2 microscope, Zeiss) together with its software (Zen 2.0, Zeiss). All histological figures were captured with a camera (AxioCam MRc5 camera, Zeiss), connected to an automatic scanning table (M-686K011, Wienecke & Sinske GmbH, Gleichen, Germany).

2.4 | Quantitative analyses

In each animal, the height of each membrane was separated into three sections of the same size (A—top layer, B—middle layer, and C—ground layer) as shown in Figure 3a. Within each section, six fields of views (size 128px × 128px) were randomly selected and analyzed. The areas of CD68-, CD11b-, αSMA-, and FGFR4-positive marked cells were calculated as sum of areas (Adobe Photoshop CS6, Adobe Systems Inc., San Jose, CA), the values were set in relation to the predefined field and the resulting mean ratio (percentage rate) was calculated for each section. Additionally, CD34 positive-marked vessels (Figure 3b,c) in each predefined field of view were counted and reported as number of vessels of each section.

2.5 | Statistics

Analyses were performed with SPSS statistical package version 20.0 (SPSS Inc., Chicago, IL). With an intended $n = 7$ per group and time, the sample size was higher as compared to other studies evaluating the biological properties of different membranes (Fujioka-Kobayashi et al., 2017; Mahajan et al., 2018; Talebi Ardakani, Hajizadeh, & Yadegari, 2018). Results were expressed as arithmetic means ± *SEM*. Before testing for statistical significances, all variables were evaluated for normal distribution via Shapiro–Wilk test. Two-way analysis of variance (ANOVA) for membranes (first way) and time (second way) followed by subsequent repeated measures within one group and analyses between four groups at each time point were conducted via ANOVA (parametric data), respectively, Kruskal–Wallis rank sum test (nonparametric data). Depending on the presence or the absence of normal distribution, Student's *t* test, respectively, Mann–Whitney test for continuous variables were used for pairwise comparison at each time point. *p*-Values <.05 were considered as significant. Bar and line charts with error bars (*SEM*) were used for data illustration.

3 | RESULTS

3.1 | Intravital vascularization analysis

For all animals ($n = 28$; $n = 7$ samples per group [homogenous dermal membrane [CM1]: $n = 7$; bilayer dermal membrane [CM2]: $n = 7$; pericardial membrane [CM3]: $n = 7$ and pericardial membrane coated with BSM [CM4]: $n = 7$]), postoperative healing was uneventful.

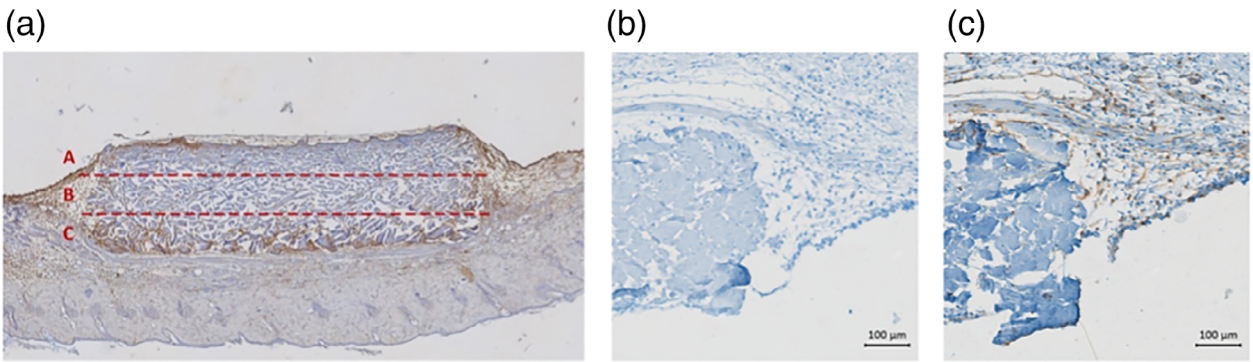

FIGURE 3 Trisection of integrated collagen membrane (a—top layer, b—middle layer, and c—ground layer) (a) and images of predefined regions with CD34 positive-marked vessels (b: negative control without any antibody and c: positive control)

Additionally, 140 intravital fluorescence microscopy video clips per region of interest (n = 7 for each group at each time point) were analyzed. In total, an increase of all vascularization parameters was seen in all CM over time (Tables 1 and 2).

3.2 | Group comparisons of intravital vascularization analysis

3.2.1 | Three days

The pericardial membrane coated with BSM (CM4) showed the highest values for capillary diameter (CDI, 11-fold); CDE (ninefold); CFL (12-fold); and CLE (ninefold) when compared to the homogenous dermal membrane (CM1; all: $p \leq .034$) and the pericardial membrane without coating (CM3; CDI: 10-fold, CDE: 30-fold, CFL: 13-fold, CLE: ninefold; all: $p \leq .029$; Figure 4; Tables 1 and 2).

3.2.2 | Six days

At this time point, CM4 also had the highest vascularization values regarding CDI (10-fold), CDE (28-fold), CFL (18-fold), and CLE (30-fold) when compared to CM1 (all: $p < .001$). The direct comparison of CM4 with CM2/CM3 showed significant higher values in all parameters (all: $p \leq .021$). Additionally, higher values of CDE, CDI, and CFL were detected in CM3 when compared to CM1 (all $p \leq .034$; Figure 4; Tables 1 and 2).

3.2.3 | Nine days

Similar to the previous time points, significant higher values in all vascularization parameters were seen in the modified pericardial (CM4) versus the homogenous dermal membrane (CM1). In brief, CDI was increased 12 times, CDE 25 times, CFL 1.5 times and CLE 12 times (all values: $p < .001$). Also, all vascularization parameters except for CLF were significantly increased in the nonmodified pericardial membrane (CM3) versus CM1 (all: $p \leq .003$) and—except for CLE—in CM3 versus the bilayer dermal membrane (all: $p \leq .031$). For CDI and CLE, higher values were found in CM4 when compared to CM3 ($p = .004$, respectively, $p = .008$; Figure 4; Tables 1 and 2).

3.2.4 | Twelve days

CM4 still showed the highest values of all groups regarding CDI (3.5-fold), CDE (33-fold), CFL (1.4-fold), and CLE (ninefold) compared to the lowest values seen for CM1 (all: $p < .001$). All vascularization parameters were also significantly lower in CM1 when compared to all other groups (all: $p \leq .003$; Figure 4; Tables 1 and 2).

3.3 | Descriptive histological analysis

All CMs were well tolerated and new blood vessels were observed. In the HE-stained samples, no hints for inflammatory reactions were found and all CMs were still visible in all groups after 12 days.

TABLE 1 Mean ± *SEM* for measurement of intravital fluorescence microscopy (all values rounded to one, respectively, two decimal digits)

Membrane	Vascularization parameter	Day 3	6	9	12	*p*-Valueb
CM1	CDI (μm)	0.09 ± 0.09	0.24 ± 0.17	1.42 ± 0.45	1.60 ± 0.50	.003
	CDE (cm/cm^2)	0.38 ± 0.38	0.50 ± 0.36	1.59 ± 0.65	3.06 ± 1.13	.004
	CFL (mm/s)	0.003 ± 0.003	0.004 ± 0.004	0.08 ± 0.04	0.08 ± 0.03	.004
	CLE (μm)	12.1 ± 12.1	15.9 ± 11.3	99.9 ± 52.4	239.9 ± 99.7	.004
CM2	CDI (μm)	0.62 ± 0.31	0.78 ± 0.31	2.40 ± 0.49	4.07 ± 0.57	<.001
	CDE (cm/cm^2)	2.78 ± 1.45	4.32 ± 2.04	14.80 ± 3.54	33.91 ± 6.06	<.001
	CFL (mm/s)	0.01 ± 0.07	0.03 ± 0.02	0.05 ± 0.02	0.09 ± 0.02	<.001
	CLE (μm)	85.0 ± 44.0	131.4 ± 61.6	413.1 ± 107.1	1,033.3 ± 190.0	<.001
CM3	CDI (μm)	0.10 ± 0.10	0.89 ± 0.33	4.08 ± 0.63	4.87 ± 0.64	<.001
	CDE (cm/cm^2)	0.11 ± 0.11	2.49 ± 1.40	10.77 ± 2.94	34.86 ± 9.03	<.001
	CFL (mm/s)	[a]	0.06 ± 0.03	0.13 ± 0.04	0.11 ± 0.03	<.001
	CLE (μm)	1.7 ± 1.7	66.5 ± 42.3	397.9 ± 99.0	1,129.4 ± 283.3	<.001
CM4	CDI (μm)	0.98 ± 0.39	2.45 ± 0.51	5.49 ± 0.66	5.15 ± 0.65	<.001
	CDE (cm/cm^2)	3.26 ± 1.45	14.79 ± 3.89	38.19 ± 6.96	69.61 ± 10.72	<.001
	CFL (mm/s)	0.04 ± 0.02	0.07 ± 0.02	0.13 ± 0.03	0.11 ± 0.02	<.001
	CLE (μm)	103.0 ± 45.7	467.1 ± 122.7	1,195.9 ± 215.4	2,184.9 ± 399.5	<.001

Abbreviations: CDE, capillary density; CDI, capillary diameter; CFL, capillary flow; CLE, capillary length.
[a]No measurable values found.
[b]Kruskal–Wallis test for differences in each group over time.

TABLE 2 Mean ± *SEM* for measurement of intravital fluorescence microscopy (all values rounded to one, respectively, two decimal digits)

		Membrane				
Day	Vascularization parameter	CM1	CM2	CM3	CM4	*p*-Valueb
3	CDI (μm)	0.09 ± 0.09	0.62 ± 0.31	0.10 ± 0.10	0.98 ± 0.39	.035
	CDE (cm/cm^2)	0.38 ± 0.38	2.78 ± 1.45	0.11 ± 0.11	3.26 ± 1.45	.035
	CFL (mm/s)	0.003 ± 0.003	0.01 ± 0.07	[a]	0.04 ± 0.02	.026
	CLE (μm)	12.1 ± 12.1	85.0 ± 44.0	1.7 ± 1.7	103.0 ± 45.7	.035
6	CDI (μm)	0.24 ± 0.17	0.78 ± 0.31	0.89 ± 0.33	2.45 ± 0.51	<.001
	CDE (cm/cm^2)	0.50 ± 0.36	4.32 ± 2.04	2.49 ± 1.40	14.79 ± 3.89	<.001
	CFL (mm/s)	0.004 ± 0.004	0.03 ± 0.02	0.06 ± 0.03	0.07 ± 0.02	<.001
	CLE (μm)	15.9 ± 11.3	131.4 ± 61.6	66.5 ± 42.3	467.1 ± 122.7	<.001
9	CDI (μm)	1.42 ± 0.45	2.40 ± 0.49	4.08 ± 0.63	5.49 ± 0.66	<.001
	CDE (cm/cm^2)	1.59 ± 0.65	14.80 ± 3.54	10.77 ± 2.94	38.19 ± 6.96	<.001
	CFL (mm/s)	0.08 ± 0.04	0.05 ± 0.02	0.13 ± 0.04	0.13 ± 0.03	<.001
	CLE (μm)	99.9 ± 52.4	413.1 ± 107.1	397.9 ± 99.0	1,195.9 ± 215.4	<.001
12	CDI (μm)	1.60 ± 0.50	4.07 ± 0.57	4.87 ± 0.64	5.15 ± 0.65	<.001
	CDE (cm/cm^2)	3.06 ± 1.13	33.91 ± 6.06	34.86 ± 9.03	69.61 ± 10.72	<.001
	CFL (mm/s)	0.08 ± 0.03	0.09 ± 0.02	0.11 ± 0.03	0.11 ± 0.02	<.001
	CLE (μm)	239.9 ± 99.7	1,033.3 ± 190.0	1,129.4 ± 283.3	2,184.9 ± 399.5	<.001

Abbreviations: CDE, capillary density; CDI, capillary diameter; CFL, capillary flow; CLE, capillary length; CM, collagen membrane.
[a]No measurable values found.
[b]Kruskal–Wallis test for differences between groups CM1, CM2, CM3, respectively, CM4 at each time point.

3.4 | Quantitative histological analyses

Analyses of immunohistochemical staining (CD68, CD11b, αSMA, FGFR4, respectively, CD34) in Sections A, B, and C did not reveal any marked differences between the sections. Therefore, data of Sections A, B, and C were summarized and mean values for each sample were generated.

The pericardial membrane coated with BSM (CM4) showed the lowest level of FGFR4-positive and CD68-positive cells when compared to the bilayer dermal membrane (CM2; $p < .001$). For CD11b, CM4 had significant higher values when compared to CM2 ($p < .001$). CM3 showed the lowest number of CD34-positive vessels when compared to the other membranes with a significant difference to CM4 (all: $p < .004$). Additionally, the highest values of αSMA-positive cells were seen in CM3 when compared to CM4 (all: $p < .04$; Table 3 and Figure 5).

4 | DISCUSSION

Whereas the beneficial effect of CMs in GBR in terms of bone regeneration has been proven in various studies, there is a lack of literature on the active effects of and within the respective membranes. In accordance, the membrane has traditionally been considered to be a passive barrier only. However, more recent research gave evidence that CMs actively promote bone formation and bone-remodeling genes (Turri et al., 2016). Therefore, the aim of the study was to examine the chronological pattern of vascularization of two porcine dermal and two porcine pericardial CMs. It was shown, that there are vast differences in the speed of vascularization over the time and the extend of vascularization at the defined endpoint. In brief, the modification of the pericardial CM with silica-enhanced nanostructured hydroxyapatite resulted in the fastest and most pronounced vascularization of all tested membranes whereas the least activity was seen for the dermal homogenous membrane. Therefore, the null hypothesis was rejected. This is in accordance to the literature showing that the addition of glass nanoparticles to resorbable membranes had a positive effect on cellular metabolic activity as well as on mineralization and bone regeneration (Hong et al., 2010; Mota et al., 2012; Tirri et al., 2008). Although to the best of our knowledge, this is the first in vivo research covering the respective evolvement over time. These different biological behaviors might influence the outcome of GBR as membranes should support an early transmembraneous angiogenesis without early degradation in order to promote osseous regeneration (Rothamel et al., 2005; Schwarz et al., 2008). In accordance, the pore size and structure of the GBR-membrane influences the degree of bone regeneration within the defect since this determines diffusion of nutrients and bioactive substances (Oh, Kim, Kim, & Lee, 2006) and a total occlusive barrier was associated with a slow bone-tissue regeneration rate (Lundgren, Lundgren, & Taylor, 1998).

Both pericardial membranes (Jason with and without NanoBone) used in this study consist of variable oriented collagen fibers creating a comb-like structure that is characterized by multidirectional linking (Elgali et al., 2017; Ortolani et al., 2015). This is different to the

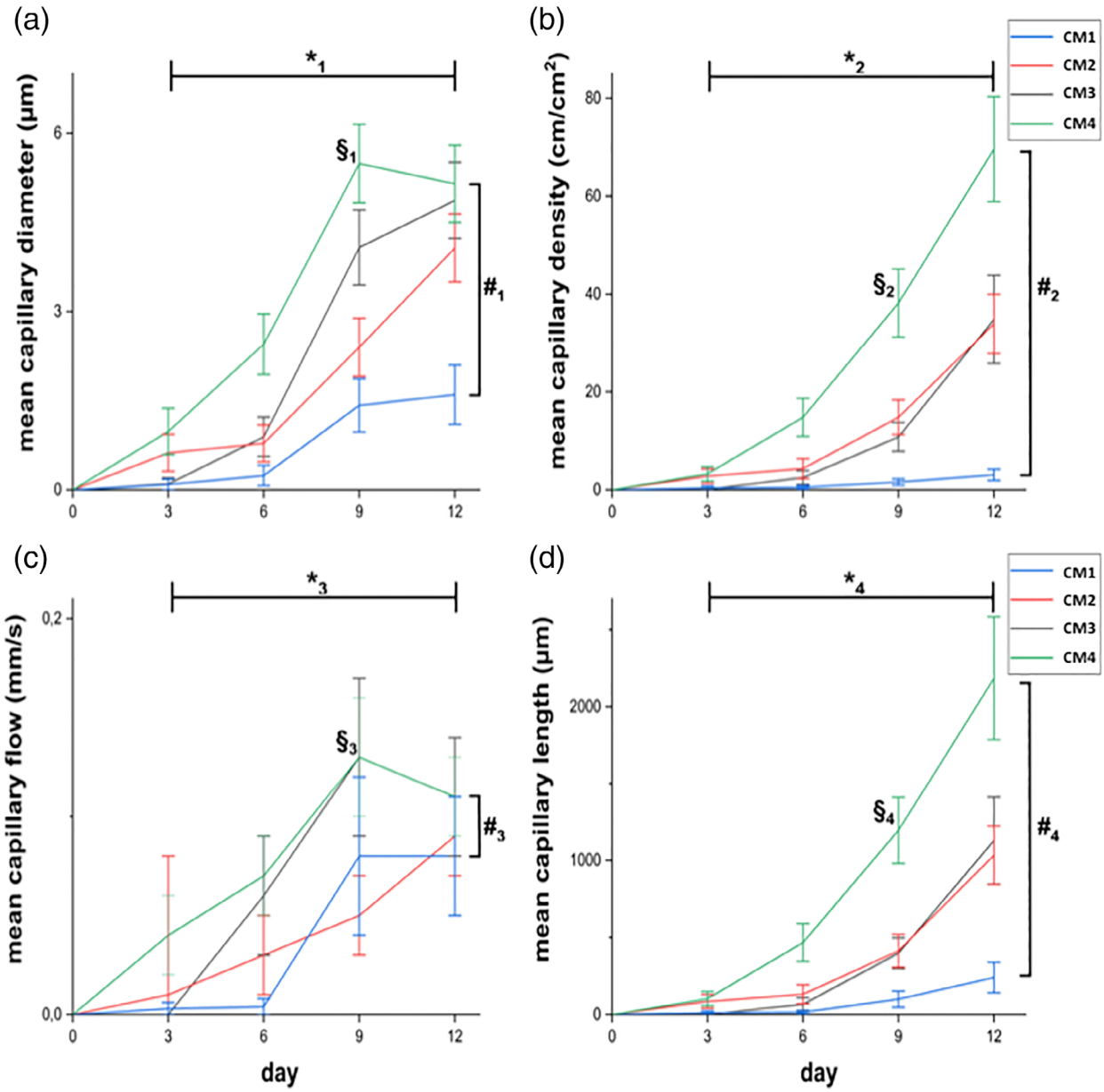

FIGURE 4 Line charts (mean percentage values including error bar presenting *SEM*) of capillary diameter (CDI) (a), capillary density (CDE) (b), capillary flow (CFL) (c), and capillary length (CLE) (d) over time (day. For details in significance, please see Table 1, respectively, Table 2

TABLE 3 Mean ± *SEM* for immunohistochemical analyses regarding FGFR4, CD11b, CD68, respectively, αSMA positive-marked cells (percentage rate; all values rounded to one decimal digit) and total number of CD34 positive-marked vessels (all values rounded to two decimal digit)

		Membrane				
Marker	Area	CM1	CM2	CM3	CM4	*p*-Valuea
FGFR4 (percentage rate)	All	3.4 ± 5.2	7.4 ± 7.6	6.6 ± 7.8	1.4 ± 1.4	<.001
CD11b (percentage rate)	All	5.1 ± 3.6	4.7 ± 3.1	7.4 ± 6.6	8.3 ± 7.2	<.001
CD68 (percentage rate)	All	2.5 ± 4.1	6.0 ± 7.5	3.5 ± 3.4	2.0 ± 1.8	<.001
αSMA (percentage rate)	All	0.8 ± 0.7	1.0 ± 0.6	1.4 ± 1.8	0.8 ± 1.1	<.001
CD34 (total number)	All	0.24 ± 0.38	0.24 ± 0.34	0.15 ± 0.26	0.45 ± 0.67	<.001

Abbreviations: CDE, capillary density; CDI, capillary diameter; CFL, capillary flow; CLE, capillary length; CM, collagen membrane; FGFR4, fibroblast growth factor receptor 4.

[a]Kruskal–Wallis test for differences between groups CM1, CM2, CM3, respectively, CM4.

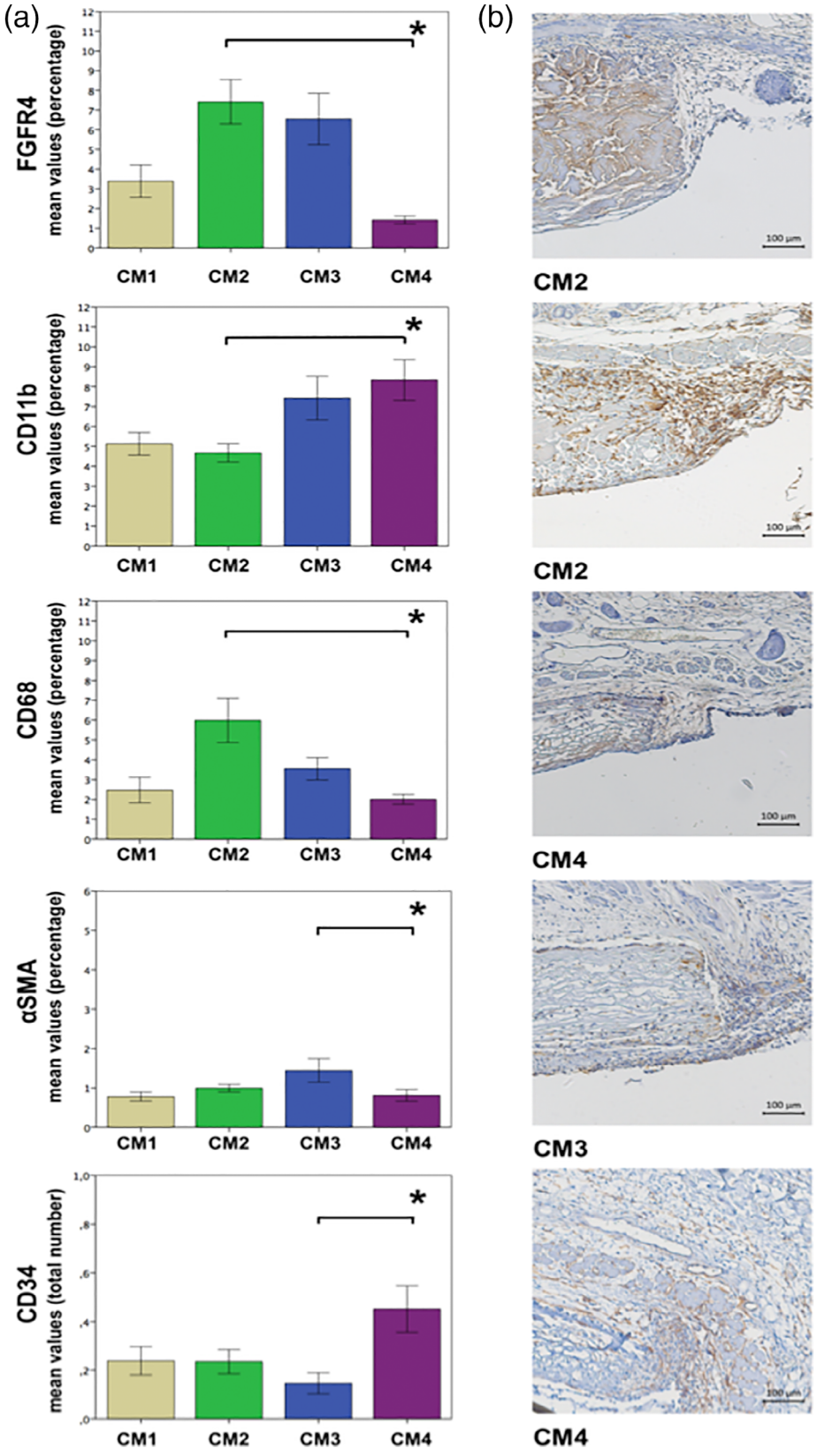

FIGURE 5 Bar chart of mean ratio (percentage) of fibroblast growth factor receptor 4 (FGFR4), CD11b, CD68, and αSMA positive-marked cell areas, respectively, mean value (total number) of CD34 positive-marked vessels (a) and selected image sections with respective immunohistochemical staining in area of collagen membrane (CM) (b); *$p < .001$

homogenous dermal derived CM 1 (Collprotect) with an open porous and three-dimensional structure and the dermal derived CM 2 (Bio-Gide) with a bilayered structure consisting of a compact and a spongy layer. Nevertheless, all CMs showed an increasing vascularization over time, even if there were differences over the time. Whereas the dermal membrane with bilayer structure and the nonmodified pericardial membrane started to have a significant increase of intravital vascularization parameters at Day 6, a notable delay of vascularization in the

homogenous CM was detected. This is supported by increased FGFR4- and αSMA-values when compared to the homogenous dermal membrane. Analogue to this, significant differences in angiogenetic pattern were described between various CMs already (Schwarz et al., 2006), even though these results were based on immunohistomorphometrical analyses only. In contrast to these findings only a mild vascularization of the porcine dermal bilayer membrane was seen within 6 weeks in a subcutaneous animal model (Ghanaati, 2012), that could be attributed to the different test approach.

In the present study, an increase of CD68-positive cells and an increase of other vascularization parameters were seen in the dermal bilayer and in the nonmodified pericardial membrane. When compared to the homogenous dermal membrane with significant lower vascularization parameters, this might indicate an association between vascularization and reorganization events.

The porcine pericardial membrane coated with synthetic BSM showed even higher vascularization parameters starting earlier at Day 3 even if CD68-values after 12 days were lower when compared to the dermal bilayer membrane. Together with the lower expression of FGFR4 and higher numbers CD34-marked vessels, this might be an indication for a combination of faster vascularization and faster reorganization.

Modification of a CM with a BSM may possibly enhance the respective mechanical properties (Anderud et al., 2014; Chu, Deng, Man, & Qu, 2017) and there is evidence for a beneficial influence of such a membrane on promotion of bone regeneration (Chu et al., 2017; Li et al., 2011; Teng et al., 2009). In accordance, this material might improve known success factors of barrier membranes in GBR such as space maintaining capacity, cell occlusiveness and bioactivation of friendly materials (Caballe-Serrano et al., 2018). As angiogenesis and vascularization is known to be central for successful GBR-procedures, its improvement is crucial for an enhanced bone regeneration. Even so, the clinical impact of such a modification should be analyzed in future research in order to optimize the biological behavior of CMs and to identify optimal material combinations.

5 | CONCLUSION

Structural different CMs from porcine origin show different biological behaviors in terms of vascularization over time. In accordance, CMs of dermal origin with a bilayer structure as well as from pericardial origin were associated with a faster vascularization when compared to homogenous CMs. Additional spraying of a pericardial CM with a silicium dioxide enriched nanostructured synthetic hydroxyapatite significantly increased diameter, density and length of surrounding vessels over time. Together with the observed high levels of CD11b and CD34 marked vessels as well as a low amount of FGFR4, this might be a hint for an even faster vascularization and biological remodeling process.

ACKNOWLEDGMENTS

The authors thank Cornelia Ganz for providing the modified CMs used in the experiment and Daniel Wolter for excellent technical assistance. This research received a specific grant from DGI (Deutsche Gesellschaft für Implantologie im Zahn-, Mund- und Kieferbereich e. V., Munich, Germany). No additional funding was made.

CONFLICT OF INTEREST

The authors declare that they have no conflict of interests and financial interests related to any products involved in this study.

ETHICS STATEMENT

All applicable international, national, and/or institutional guidelines for the care and use of animals were followed.

ORCID

Peer W. Kämmerer https://orcid.org/0000-0002-1671-3764

REFERENCES

Abshagen, K., Schrodi, I., Gerber, T., & Vollmar, B. (2009). In vivo analysis of biocompatibility and vascularization of the synthetic bone grafting substitute NanoBone. *Journal of Biomedical Materials Research. Part A*, *91*, 557–566.

Adam, M., Ganz, C., Xu, W., Sarajian, H. R., Gotz, W., & Gerber, T. (2014). In vivo and in vitro investigations of a nanostructured coating material—A preclinical study. *International Journal of Nanomedicine*, *9*, 975–984.

Amorfini, L., Migliorati, M., Signori, A., Silvestrini-Biavati, A., & Benedicenti, S. (2014). Block allograft technique versus standard guided bone regeneration: A randomized clinical trial. *Clinical Implant Dentistry and Related Research*, *16*, 655–667.

Anderud, J., Jimbo, R., Abrahamsson, P., Isaksson, S. G., Adolfsson, E., Malmstrom, J., … Wennerberg, A. (2014). Guided bone augmentation using a ceramic space-maintaining device. *Oral Surgery, Oral Medicine, Oral Pathology, Oral Radiology*, *118*, 532–538.

Blatt, S., Burkhardt, V., Kämmerer, P. W., Pabst, A. M., Sagheb, K., Heller, M., … Schiegnitz, E. (2020). Biofunctionalization of porcine-derived collagen matrices with platelet rich fibrin: Influence on angiogenesis in vitro and in vivo. *Clinical Oral Investigations*. [Epub ahead of print].

Bunyaratavej, P., & Wang, H. L. (2001). Collagen membranes: A review. *Journal of Periodontology*, *72*, 215–229.

Caballe-Serrano, J., Munar-Frau, A., Ortiz-Puigpelat, O., Soto-Penaloza, D., Penarrocha, M., & Hernandez-Alfaro, F. (2018). On the search of the ideal barrier membrane for guided bone regeneration. *Journal of Clinical and Experimental Dentistry*, *10*, e477–e483.

Chiapasco, M., & Zaniboni, M. (2009). Clinical outcomes of GBR procedures to correct peri-implant dehiscences and fenestrations: A systematic review. *Clinical Oral Implants Research*, *20*(Suppl 4), 113–123.

Chu, C., Deng, J., Man, Y., & Qu, Y. (2017). Evaluation of nanohydroxyapaptite (nano-HA) coated epigallocatechin-3-gallate (EGCG) cross-linked collagen membranes. *Materials Science & Engineering. C, Materials for Biological Applications*, *78*, 258–264.

Dau, M., Kämmerer, P. W., Henkel, K. O., Gerber, T., Frerich, B., & Gundlach, K. K. (2016). Bone formation in mono cortical mandibular critical size defects after augmentation with two synthetic nanostructured and one xenogenous hydroxyapatite bone substitute—In vivo animal study. *Clinical Oral Implants Research*, *27*, 597–603.

De Vriese, A. S., Verbeuren, T. J., Vallez, M. O., Lameire, N. H., De Buyzere, M., & Vanhoutte, P. M. (2000). Off-line analysis of red blood cell velocity in renal arterioles. *Journal of Vascular Research*, *37*, 26–31.

Elgali, I., Omar, O., Dahlin, C., & Thomsen, P. (2017). Guided bone regeneration: Materials and biological mechanisms revisited. *European Journal of Oral Sciences*, *125*, 315–337.

Fujioka-Kobayashi, M., Schaler, B., Shirakata, Y., Nakamura, T., Noguchi, K., Zhang, Y., & Miron, R. J. (2017). Comparison of two

porcine collagen membranes combined with rhBMP-2 and rhBMP-9 on osteoblast behavior in vitro. *The International Journal of Oral & Maxillofacial Implants*, *32*, e221–e230.

Ghanaati, S. (2012). Non-cross-linked porcine-based collagen I-III membranes do not require high vascularization rates for their integration within the implantation bed: A paradigm shift. *Acta Biomaterialia*, *8*, 3061–3072.

Ghanaati, S., Barbeck, M., Lorenz, J., Stuebinger, S., Seitz, O., Landes, C., … Sader, R. A. (2013). Synthetic bone substitute material comparable with xenogeneic material for bone tissue regeneration in oral cancer patients: First and preliminary histological, histomorphometrical and clinical results. *Annals of Maxillofacial Surgery*, *3*, 126–138.

Hong, K. S., Kim, E. C., Bang, S. H., Chung, C. H., Lee, Y. I., Hyun, J. K., … Kim, H. W. (2010). Bone regeneration by bioactive hybrid membrane containing FGF2 within rat calvarium. *Journal of Biomedical Materials Research. Part A*, *94*, 1187–1194.

Kämmerer, P. W., Palarie, V., Schiegnitz, E., Nacu, V., Draenert, F. G., & Al-Nawas, B. (2013). Influence of a collagen membrane and recombinant platelet-derived growth factor on vertical bone augmentation in implant-fixed deproteinized bovine bone—Animal pilot study. *Clinical Oral Implants Research*, *24*, 1222–1230.

Kämmerer, P. W., Scholz, M., Baudisch, M., Liese, J., Wegner, K., Frerich, B., & Lang, H. (2017). Guided bone regeneration using collagen scaffolds, growth factors, and periodontal ligament stem cells for treatment of peri-implant bone defects in vivo. *Stem Cells International*, *2017*, 3548435.

Keestra, J. A., Barry, O., Jong, L., & Wahl, G. (2016). Long-term effects of vertical bone augmentation: A systematic review. *Journal of Applied Oral Science*, *24*, 3–17.

Kilkenny, C., Browne, W. J., Cuthill, I. C., Emerson, M., & Altman, D. G. (2010). Improving bioscience research reporting: The ARRIVE guidelines for reporting animal research. *Journal of Pharmacology and Pharmacotherapeutics*, *1*, 94–99.

Klyscz, T., Junger, M., Jung, F., & Zeintl, H. (1997). Cap image—A new kind of computer-assisted video image analysis system for dynamic capillary microscopy. *Biomedizinische Technik. Biomedical Engineering*, *42*, 168–175.

Koerdt, S., Ristow, O., Wannhoff, A., Kubler, A. C., & Reuther, T. (2014). Expression of growth factors during the healing process of alveolar ridge augmentation procedures using autogenous bone grafts in combination with GTR and an anorganic bovine bone substitute: An immunohistochemical study in the sheep. *Clinical Oral Investigations*, *18*, 179–188.

Kyyak, S., Blatt, S., Pabst, A., Thiem, D., Al-Nawas, B., & Kämmerer, P. W. (2020). Combination of an allogenic and a xenogenic bone substitute material with injectable platelet-rich fibrin—A comparative in vitro study. *Journal of Biomaterials Applications*, 088532822091440. [Epub ahead of print].

Li, J., Man, Y., Zuo, Y., Zhang, L., Huang, C., Liu, M., & Li, Y. (2011). In vitro and in vivo evaluation of a nHA/PA66 composite membrane for guided bone regeneration. *Journal of Biomaterials Science. Polymer Edition*, *22*, 263–275.

Liu, J., & Kerns, D. G. (2014). Mechanisms of guided bone regeneration: A review. *The Open Dentistry Journal*, *8*, 56–65.

Lundgren, A., Lundgren, D., & Taylor, A. (1998). Influence of barrier occlusiveness on guided bone augmentation. An experimental study in the rat. *Clinical Oral Implants Research*, *9*, 251–260.

Mahajan, R., Khinda, P., Shewale, A., Ghotra, K., Bhasin, M. T., & Bhasin, P. (2018). Comparative efficacy of placental membrane and healiguide in treatment of gingival recession using guided tissue regeneration. *Journal of Indian Society of Periodontology*, *22*, 513–522.

Mota, J., Yu, N., Caridade, S. G., Luz, G. M., Gomes, M. E., Reis, R. L., … Mano, J. F. (2012). Chitosan/bioactive glass nanoparticle composite membranes for periodontal regeneration. *Acta Biomaterialia*, *8*, 4173–4180.

Naenni, N., Schneider, D., Jung, R. E., Husler, J., Hammerle, C. H. F., & Thoma, D. S. (2017). Randomized clinical study assessing two membranes for guided bone regeneration of peri-implant bone defects: Clinical and histological outcomes at 6 months. *Clinical Oral Implants Research*, *28*, 1309–1317.

Oh, S. H., Kim, J. H., Kim, J. M., & Lee, J. H. (2006). Asymmetrically porous PLGA/Pluronic F127 membrane for effective guided bone regeneration. *Journal of Biomaterials Science. Polymer Edition*, *17*, 1375–1387.

Ortolani, E., Quadrini, F., Bellisario, D., Santo, L., Polimeni, A., & Santarsiero, A. (2015). Mechanical qualification of collagen membranes used in dentistry. *Annali dell'Istituto Superiore di Sanità*, *51*, 229–235.

Pabst, A., & Kämmerer, P. W. (2020). Collagen matrices: Opportunities and perspectives in oral hard and soft tissue regeneration. *Quintessence International*, *51*, 318–327.

Park, J. S., Pabst, A. M., Ackermann, M., Moergel, M., Jung, J., & Kasaj, A. (2018). Biofunctionalization of porcine-derived collagen matrix using enamel matrix derivative and platelet-rich fibrin: Influence on mature endothelial cell characteristics in vitro. *Clinical Oral Investigations*, *22*, 909–917.

Rothamel, D., Benner, M., Fienitz, T., Happe, A., Kreppel, M., Nickenig, H. J., & Zoller, J. E. (2014). Biodegradation pattern and tissue integration of native and cross-linked porcine collagen soft tissue augmentation matrices—An experimental study in the rat. *Head & Face Medicine*, *10*, 10.

Rothamel, D., Schwarz, F., Sager, M., Herten, M., Sculean, A., & Becker, J. (2005). Biodegradation of differently cross-linked collagen membranes: An experimental study in the rat. *Clinical Oral Implants Research*, *16*, 369–378.

Schwarz, F., Rothamel, D., Herten, M., Sager, M., & Becker, J. (2006). Angiogenesis pattern of native and cross-linked collagen membranes: An immunohistochemical study in the rat. *Clinical Oral Implants Research*, *17*, 403–409.

Schwarz, F., Rothamel, D., Herten, M., Wustefeld, M., Sager, M., Ferrari, D., & Becker, J. (2008). Immunohistochemical characterization of guided bone regeneration at a dehiscence-type defect using different barrier membranes: An experimental study in dogs. *Clinical Oral Implants Research*, *19*, 402–415.

Sckell, A., & Leunig, M. (2009). The dorsal skinfold chamber: Studying angiogenesis by intravital microscopy. *Methods in Molecular Biology*, *467*, 305–317.

Sckell, A., & Leunig, M. (2016). Dorsal skinfold chamber preparation in mice: Studying angiogenesis by intravital microscopy. *Methods in Molecular Biology*, *1430*, 251–263.

Shim, J. H., Huh, J. B., Park, J. Y., Jeon, Y. C., Kang, S. S., Kim, J. Y., … Cho, D. W. (2013). Fabrication of blended polycaprolactone/poly(lactic-co-glycolic acid)/beta-tricalcium phosphate thin membrane using solid freeform fabrication technology for guided bone regeneration. *Tissue Engineering. Part A*, *19*, 317–328.

Silva, E. C., Omonte, S. V., Martins, A. G., de Castro, H. H., Gomes, H. E., Zenobio, E. G., … Souza, P. E. (2017). Hyaluronic acid on collagen membranes: An experimental study in rats. *Archives of Oral Biology*, *73*, 214–222.

Talebi Ardakani, M. R., Hajizadeh, F., & Yadegari, Z. (2018). Comparison of attachment and proliferation of human gingival fibroblasts on different collagen membranes. *Annals of Maxillofacial Surgery*, *8*, 218–223.

Teng, S. H., Lee, E. J., Yoon, B. H., Shin, D. S., Kim, H. E., & Oh, J. S. (2009). Chitosan/nanohydroxyapatite composite membranes via dynamic filtration for guided bone regeneration. *Journal of Biomedical Materials Research. Part A*, *88*, 569–580.

Tirri, T., Rich, J., Wolke, J., Seppala, J., Yli-Urpo, A., & Narhi, T. O. (2008). Bioactive glass induced in vitro apatite formation on composite GBR membranes. *Journal of Materials Science. Materials in Medicine*, *19*, 2919–2923.

Turri, A., Elgali, I., Vazirisani, F., Johansson, A., Emanuelsson, L., Dahlin, C., … Omar, O. (2016). Guided bone regeneration is promoted by the molecular events in the membrane compartment. *Biomaterials*, *84*, 167–183.

SUPPORTING INFORMATION

Additional supporting information may be found online in the Supporting Information section at the end of this article.

How to cite this article: Dau M, Volprich L, Grambow E, et al. Collagen membranes of dermal and pericardial origin—In vivo evolvement of vascularization over time. *J Biomed Mater Res*. 2020;108:2368–2378. https://doi.org/10.1002/jbm.a.36989